Received: 14 February 2016 ■ *Revised: 8 October 2016* ■ *Accepted: 19 October 2016* ■ *Publication: 18 November 2016*

JNIRS JOURNAL OF NEAR INFRARED SPECTROSCOPY

Special Issue: Wood and Wood Products

openaccess

Near infrared hyperspectral imaging in transmission mode: assessing the weathering of thin wood samples

Knut Arne Smeland,[a] Kristian Hovde Liland,[b] Jakub Sandak,[c] Anna Sandak,[c] Lone Ross Gobakken,[d] Thomas Kringlebotn Thiis[a] and Ingunn Burud[a]*

[a]Norwegian University of Life Sciences, Department of Mathematical Sciences and Technology, Campus Ås, Pb 5003, 1430 Ås, Norway. E-mail: ingunn.burud@nmbu.no

[b]Nofima-Norwegian Institute of Food, Fisheries and Aquaculture Research, Pb 210, NO-1430 Ås, Norway

[c]Trees and Timber Institute IVALSA/CNR, via Biasi 75, 38010 San Michele all'Adige (TN), Italy

[d]Norwegian Institute of Bioeconomy Research, Pb 115, NO-1431 Ås, Norway

Untreated wooden surfaces degrade when exposed to natural weathering. In this study thin wood samples were studied for weather degradation effects utilising a hyperspectral camera in the near infrared wavelength range in transmission mode. Several sets of samples were exposed outdoors for time intervals from 0 days to 21 days, and one set of samples was exposed to ultraviolet (UV) radiation in a laboratory chamber. Spectra of earlywood and latewood were extracted from the hyperspectral image cubes using a principal component analysis-based masking algorithm. The degradation was modelled as a function of UV solar radiation with four regression techniques, partial least squares, principal component regression, Ridge regression and Tikhonov regression. It was found that all the techniques yielded robust prediction models on this dataset. The result from the study is a first step towards a weather dose model determined by temperature and moisture content on the wooden surface in addition to the solar radiation.

Keywords: hyperspectral imaging, regression models, wood weathering, degradation kinetic

Introduction

The use of wood outdoors is widespread in a variety of applications, one of them being as claddings on building façades. Untreated wood is nowadays frequently utilised as cladding in modern buildings, and there is a trend towards less surface treatment of the wood to obtain a naturally weathered result. Ensuring the optimal choice of wood species requires a thorough understanding of the deterioration mechanisms of wood during outdoor exposure. While it is known that the characteristic grey patina visible after a few months of exposure is mostly caused by photodegradation of lignin in the middle lamella by ultraviolet (UV) radiation,[1] there are several other factors involved, such as humidity, temperature, biological growth, chemical and mechanical abrasion.[2] The elements used in façades made of wood can often cause a non-uniform degradation pattern such as shown in Figure 1. Various architectural solutions, such as the location of windows, overhangs etc. induce specific discoloration patterns, since these affect the microclimate on the surface. This is because the microclimate underneath a roof overhang is different from that on an open façade, which again is different from one under a window.

The microclimate at each point of a wooden façade can be modelled from the exterior climate using ray tracing to account

ISSN: 0967-0335
doi: 10.1255/jnirs.1253

Figure 1. Unevenly weather-exposed wooden surface on a building façade, Aas, Norway.

for micro-scale variation in the solar irradiance, temperature and moisture on the wall, as presented in Thiis *et al*.[3]

In order to foresee the degradation on the different parts of a wall, accurate prediction models of wood degradation as a function of the main climatic factors are important.

Near infrared (NIR) spectroscopy and hyperspectral imaging are well-suited scientific tools for rapid and non-destructive characterisation of wood surfaces.[4,5] A review of different band assignments for NIR spectroscopy on wood was written by Schwanninger *et al*.[6] An advantage of these techniques is the possibility of determining both chemical and physical properties of a large number of samples.

The goal of this study was to assess the degradation of wood due to weathering, and to model degradation kinetics based on thin wood samples, exposed outdoors, by means of NIR hyperspectral imaging. The study has focused on the influence of UV radiation on the weathering of wood and its perceptibility in NIR spectral images of the exposed wood samples. According to Grossman,[7] a widely used practice has been to use total energy (Joules) from the integrated solar spectrum as the timing variable for the amount of radiation a sample has been exposed to. This is obtained by integrating over the entire spectral power curve of sunlight, and multiplying by exposure time.[1] Here, this approach is built upon by comparing results from partial least squares (PLS) and principal component regression (PCR), with results obtained using Tikhonov regularisation.[8] After accounting for the materials and equipment used, the pre-processing procedures will be presented as well as details on the statistical analysis, with a particular focus on the Tikhonov regularisation method.

Materials and methods

Sample preparation

Experimental samples were prepared from one piece of Norway spruce wood (*Picea abies*) on a slicing planner (Super meca, Marunaka, Japan) to a thickness of ~100 µm, and an effective surface exposed of 30 × 35 mm. A total of 105 samples were exposed outdoors in Ås, Norway, facing south at 45° as shown in Figure 2 (left). On the first day, 21 samples were placed outside for exposure, and then one sample was collected each day and stored at room temperature. After 7 days a new set of 21 samples were exposed, and on the following days one sample was collected each day following the same procedure as for sample set 1. This procedure was followed for 5 sample sets of 21 samples each. After collecting all samples they were stored in darkness in a climatic chamber with a constant temperature of 20°C and 65% relative humidity to obtain an

Figure 2. Left: samples exposed outdoors facing south. Right: samples from different sample sets exposed for 1 (no. 45), 10 (no. 93) and 20 (no. 104) days.

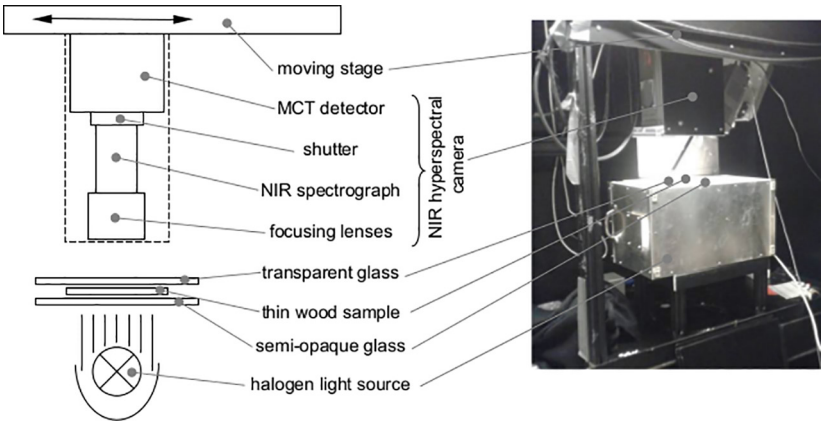

Figure 3. Hyperspectral imaging setup in transmission mode.

acclimatised weight before further processing. Three samples from different sample sets are shown in Figure 2 (right) and demonstrate the colour change due to various outdoor exposure times. Weather data for the location was obtained from a national weather station located approximately 200 m away from the exposure site. The weather station has a pyranometer that measures the solar UV radiation in the wavelength region (298–385 nm), which was used as the response value when modelling the wood degradation from the NIR spectra.

A supplementary set of 30 samples were exposed in a UV chamber (Atlas UVTest). The Atlas UVTest has eight UVA-340 lamps, with an output of 0.89 $W m^{-2} nm^{-1}$ at 340 nm each. The samples were exposed in the UV chamber for 1–10 cycles of 2.5 h continuous UV radiation followed by 0.5 h water spraying.

Chemical composition

A subset of the samples from each exposure group (outdoor exposed samples and UV chamber exposed samples) were analysed with a simultaneous thermal analyser coupled with Fourier transform infrared (FT-IR) spectrometer (STA FF9 F1 Jupiter, NETSCH, Germany) to estimate the lignin and holocellulose (cellulose + hemicellulose) content. The samples on which this measurement was performed had all been placed outside on the same day so that they are from one series of time exposure. In order to have separated lignin and holocellulose estimates for early- and latewood the samples had to be cut into pieces of each. Since the early- and latewood are separated by a few millimetres this task was performed with a scalpel. The samples were laid on a white background and the pieces of early- and latewood were cut in the directon of the fibres. The pieces of early- and latewood were then put in small containers for the thermal analyser. There was only enough material to perform one early- and latewood measurement of each sample.

Spectral imaging and pre-processing

Hyperspectral images were obtained using a linescan camera with a spectral resolution of resolution of 6 nm (256 bands) and a spatial resolution of 320 pixels with a mercury cadmium telluride detector having spectral sensitivity in the 929–2531 nm range (SWIR-LVDS-100-N25E, Specim, Oulu, Finland, www.specim.fi). The hyperspectral image acquisition was carried out in transmission mode using a custom setup (Figure 3). This consisted of backside illumination with halogen lamps below a semi-opaque glass plate, and another transparent glass plate transmitting NIR radiation above the samples. At the end of the scan of each sample, a short image with the shutter closed is taken and the mean signal from each line in this dark image is subtracted from each band in the hypercube. This procedure is performed to remove the bias level and to correct for pixel to pixel variations in the detector. A white calibration has to be performed in order to remove the spectral signal from the lamps. However, a regular white calibration Spectralon plate cannot be used in transmission mode. To obtain the white calibration, an image of the empty glass plate was therefore used so that all the sample images were divided by this image after subtraction of the dark signal. The dark subtraction and the white calibration can be formulated mathematically as in Equation 1.

$$I_{corr} = (I_{raw} - \bar{D}) / W_{raw} - \bar{D}) \quad (1)$$

where I is the image frame, D is the dark image and W is the white calibration image.

The earlywood and latewood parts can be identified on the hyperspectral images. In order to automatically extract mean spectra from the earlywood and latewood parts of the samples, a threshold mask based on principal component analysis (PCA) was applied to the images. After performing PCA on a selection of the images, it was found that the distinction between earlywood and latewood was best represented in the second component of the PCA. Score images from this component were therefore used as references for the threshold. Early wood areas of these images were characterised by low score values and late wood by high score values, but the ranges varied from image to image. To compensate for varying ranges, quantiles were used for the threshold instead of absolute values. The lower 0.25 and the upper 0.35 quantiles proved to be suitable, as shown schematically in Figure 4.

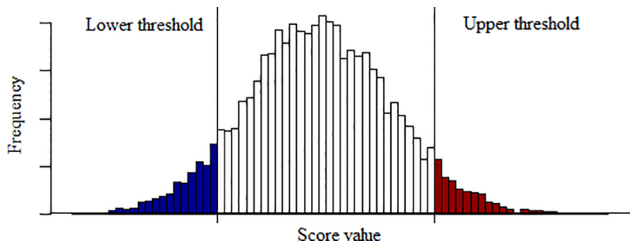

Figure 4. Schematic drawing of how the lower 0.25 and the upper 0.35 quantiles of the PCA score values were selected to represent early- and latewood.

The earlywood and latewood masks were then updated to include only pixels with scores in those quantiles, respectively.

The recorded transmission spectra were transformed to absorbance using a log10 transformation procedure. A few of the spectra contain some "dead" wavelengths with intensities of 0. Since $\log_{10}(0) = 1$, this caused problems further on when analysing the spectra. This was remedied by applying a spike removal procedure (htdeadwavelengths from the Hypertools package, http://www.models.life.ku.dk/HYPERTools). The ten first and the last ten wavelength bands were also excluded from the spectra, since they contain random signals associated with noise.

Since the electromagnetic spectrum is continuous and the signal at one wavelength is strongly correlated with signals at proximate wavelengths, one can conclude that an ideal spectrum should display continuity between neighbouring wavelengths. However, various instrumental influences perturb the actual signal. Whereas the validity of the data points cannot be concluded without further investigation, an *a priori* knowledge permits the use of a set of tools to remove some of this noise before any further analysis is performed,[9] improving the signal-to-noise ratio. The simplest of these is calculating a moving average over the whole spectrum. Moving average techniques can have the undesired effect of smoothing peaks in the spectra, particularly shoulders and reducing their intensity, which may result in removal of meaningful information.[9] As an improvement, Savitzky and Golay[9] proposed an alternative solution based on the method of least squares, which was used in this work. The ideal window size of the moving average depends on the wavelength resolution, and in this case a window size of nine pixels was found to produce the best results. The model used was a second-degree polynomial, without derivatives. An illustration of the effect is shown in Figure 5.

In order to study the chemical makeup of the samples most successfully, it is important to separate the physical variation from the chemical. One of the most meritorious of the available methods to accomplish this is the (Extended) multiplicative signal correction, or (E)MSC.[10] The basic idea of MSC is to fit a regression model of all the spectra in an image to an ideal (reference) spectrum and a flat baseline, and then use the coefficients to perform the correction. EMSC is an extension of MSC that includes terms that account for variation such as differences in scattering over different wavelengths.[11,12] In this work, a model with parameters for wavelength and squared wavelength was used, so the model can be written as:

$$\mathbf{z}_{observed} = \alpha + \beta_1 \mathbf{m} + \beta_2 \lambda + \beta_3 \lambda^2 \quad (2)$$

where $\mathbf{z}_{observed}$ is the observed absorbance spectrum, α the baseline offset, β the scaling parameters and λ the wavelength. The mean spectrum of the sample, $\mathbf{m}$, is used as a

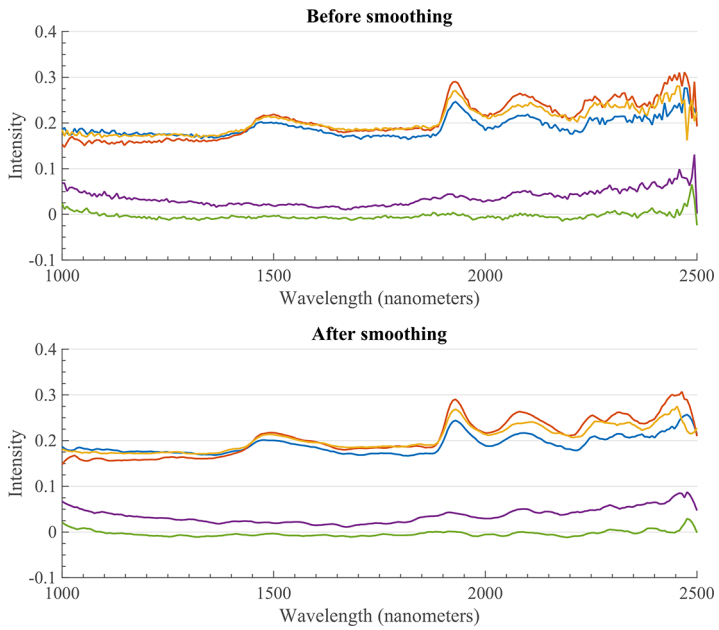

Figure 5. Ten random pixels from an arbitrarily selected image before (top) and after (bottom) Savitzky–Golay smoothing with a window size of nine pixels.

reference spectrum for the correction. This correction was performed for all the spectra in all the samples using the HySpec Toolbox (Liland *et al.*, http://nofimaspectroscopy.org).

After pre-processing, it was noted that parts of the spectra had a very distinct feature at 1850 nm. The spectra were captured from samples that had been stored in a separate envelope. It was concluded that this feature was due to different moisture conditions in the storage of the samples. This had affected the spectra of the samples since the samples are very thin and very sensitive to climate conditions. These samples were therefore excluded from the analysis.

Regression model development

After pre-processing was completed, the data ready for analysis consisted of four data sets which were the earlywood and latewood mean spectra for each sample in each group (outside exposure group and UV chamber group). Two approaches for regression analysis of the spectra were used to analyse the data: (a) using the mean spectra of early and latewood separately as predictor variables and the number of days/cycles of exposure as the response variable and (b) using weather data from the period to calculate UV solar radiation for each sample as response variable. The set of predictor variables and the response variable are all continuous, and so the point of departure is Ordinary Least Squares Regression, of the familiar form: $\mathbf{y} = \beta_0 + \beta_{1\times1} + \ldots + \beta_n x_n + \varepsilon$. Here β_0 is the expected value when all $\mathbf{x} = 0$, β_1, …, β_n are the coefficients associated with each variable and ε is the error term representing variation not accounted for by the model. In linear algebra notation the data can be arranged as:[13]

$$\mathbf{X}\beta = \mathbf{y} + \varepsilon \tag{3}$$

where the rows of **X** correspond to observations and the columns correspond to variables, with a vector of ones added to account for the constant term. β is a vector containing the regression coefficients and **y** is the response vector. The aim of the regression is to derive a model that predicts new observations accurately and reliably. Given an observation with response y from a population with an unknown mean μ, an associated explanatory variable x and an estimate of y given by some function $\hat{y} = f(x)$ Then the mean squared error (*MSE*) of $\hat{y}$ is given by Equation 4:

$$MSE(\hat{y}) = E\left[y - f(x)\right]^2 = E(y-\mu)^2 + \left[\mu - f(x)\right]^2 \tag{4}$$

where $E(y-\mu)^2$ represents the variance $Var(y)$ and $[\mu - f(x)]^2$ the $bias^2$. This is known as the bias–variance decomposition[14] and the minimisation of this is a trade-off between increasing the model complexity or the model robustness. With an increased model complexity the bias can be decreased, but the variance will increase. Such a complex model may predict well for the set on which it was trained, but it might not generalise well to new data.[14] By relaxing the requirement that the model should be unbiased, it is possible to obtain a model that has stronger predictive power, by finding the optimal trade-off between bias and variance.[15] The method we have chosen for doing this is adding a regularisation term to the least squares estimator. In particular we use Tikhonov regularisation.[8] In the special case where the regularisation term is the identity matrix, the method is also called ridge regression. The variables in a hyperspectral image are often highly correlated, because one wavelength will have values similar to its neighbouring wavelengths. This can make the data matrix severely ill-conditioned[16] in the way that the least squares solution will be very sensitive to perturbations in the data, such as those stemming from measurement errors.[15] Since these are common in hyperspectral imaging, the model should be resistant to such perturbations. The goal in regularising the data is to shrink this vector of coefficients, β, so it is more resilient to small variations in the data matrix **X**. The effect of increasing the value of the regularisation parameter is to reduce the fluctuations in the β vector. If the regularising parameter value is very high, the curve of β coefficients would end up as a straight line, in which case none of the variables would have any effect on the outcome. So there are two objectives: keeping $01 = ||\mathbf{X}\beta - \mathbf{y}||^2$ small, and keeping $02 = ||\mathbf{F}\beta - \mathbf{g}||^2$ small. When $\mathbf{F} = \mathbf{I}$ and $\mathbf{g} = 0$, this corresponds to keeping $02 = ||\beta||^2$ small, that is, putting more weight on objective 2 emphasising shrinking of the coefficient vector. The expression of this weighted-sum objective is

$$\mathbf{X}\beta - y^2 + \lambda\mathbf{F}\beta - \mathbf{g}^2 = \left[\begin{matrix}\mathbf{X}\\ \sqrt{\lambda}\,\mathbf{F}\end{matrix}\right]\beta - \left[\begin{matrix}\mathbf{y}\\ \sqrt{\lambda}\,\mathbf{g}\end{matrix}\right]^2 = \mathbf{X}\beta - \mathbf{y}^2 \tag{5}$$

Table 1. Lignin measurements from the STA-FT-IR analysis. The standard deviation of the lignin is 0.23%, based on reference measurements. The three control samples were not exposed but remained in a dark room with controlled climate.

Days of exposure earlywood	Lignin (%)	Days of exposure latewood	Lignin (%)
0 (control #1)	25.8	0 (control #1)	28.8
0 (control #2)	26.4	0 (control #2)	29.4
0 (control #3)	25.4	0 (control #3)	25.8
2	27.9	2	27.1
3	30.2	3	24.9
5	29.7	5	28.3
6	28.8	6	27.5
8	29.3	8	27.3
9	27.5	9	29.0
11	32.2	11	27.6
12	31.0	12	26.9
14	32.8	14	27.9
15	31.6	15	29.1
17	30.1	17	28.7
19	35.5	19	29.5
20	37.6	20	28.9
21	31.7	21	26.8

Table 2: Coefficient of determination, R^2, for the models developed within this study.

	Ridge	1st d. Tikhonov	PCR-R	PLS-R
Weather, early	0.833	0.831	0.837	0.841
Weather, late	0.786	0.749	0.790	0.784
Artificial UV, early	0.784	0.743	0.793	0.781
Artificial UV, late	0.764	0.778	0.760	0.765

where

$$\mathbf{X} = \begin{bmatrix} \mathbf{X} \\ \sqrt{\lambda}\mathbf{F} \end{bmatrix}, \mathbf{y} = \begin{bmatrix} \mathbf{y} \\ \sqrt{\lambda}\mathbf{g} \end{bmatrix}$$

and λ is the weight put on objective 2, called the regularisation parameter. If λ = 0, the result is the classic least squares. As λ approaches infinity, the coefficients get "nulled" out and only the intercept (mean value) remains.[17]

In our work we used ridge regression and Tikhonov regularisation that introduced a regularisation operator that optimises with respect to the first and second derivatives of the coefficient vector.[18] In addition, PLS regression[19] and PCR[20] were performed on the same data set. As with the regularisation methods, one of the strengths of PLS regression lies in its ability to handle data that are noisy, underdetermined and highly collinear.[19]

To check the validity of the models, the datasets were split in two, with 2/3 of each dataset assigned as training data and the remaining 1/3 as test data. The observations were assigned at random and the model fitted to the training set was used to predict for the test set. In order to better assess the reliability of the method, a resampling procedure was used in which the randomised sampling was performed 1000 times, and a model fitted to each. The coefficient of determination was recorded and averaged, yielding mean values for R^2.

Results and discussion

Regression analysis

The mean values of the coefficient of determination, R^2, for the four regression methods (ridge, Tikhonov, PLS and PCR) for prediction of UV radiation are shown in Table 2. All the four techniques yield good regression fits, and none of the techniques outshines the others for these data. The coefficients vectors for the four regression methods for outdoor exposed earlywood are shown in Figure 6 illustrating that the Tikhonov first derivative has a smoother curve, and is hence expected to yield a more robust solution. However, this does not seem to have any impact on the fit for this dataset.

The mean predicted values versus measured values for each data point of the outdoor exposed samples are plotted in Figures 7 and 8 for earlywood and latewood, respectively. Also shown are histograms of the R^2 values for the 1000 model runs.

The results for the samples from the UV chamber are shown in Figures 9 and 10 for earlywood and latewood, respectively. A ridge regression model that was calibrated on the samples exposed to the UV radiation chamber applied to predict the weather-exposed samples is shown in Figure 11. It can be

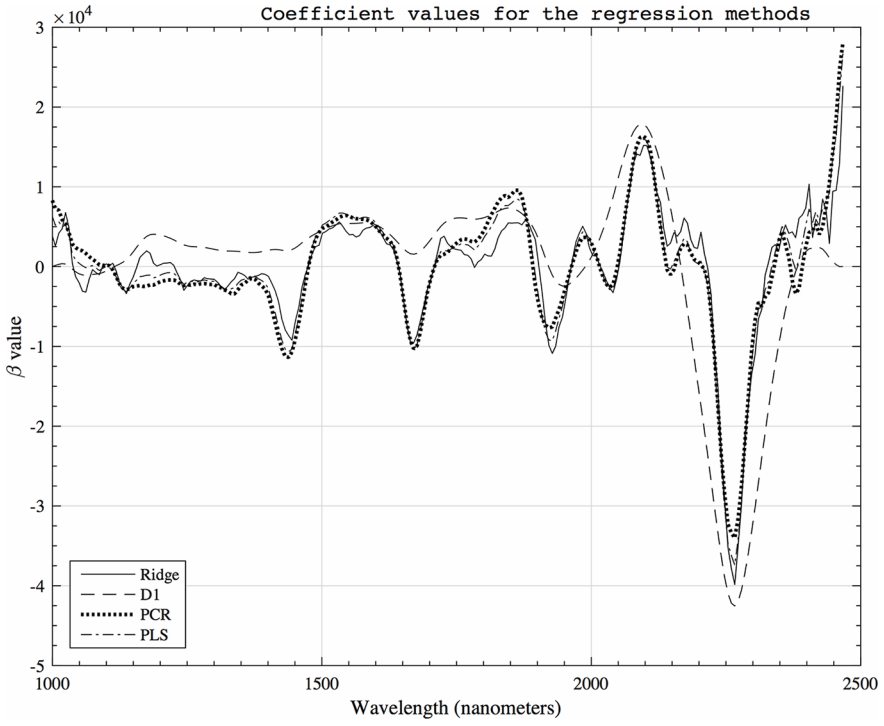

Figure 6. Coefficient vectors for the different regression methods.

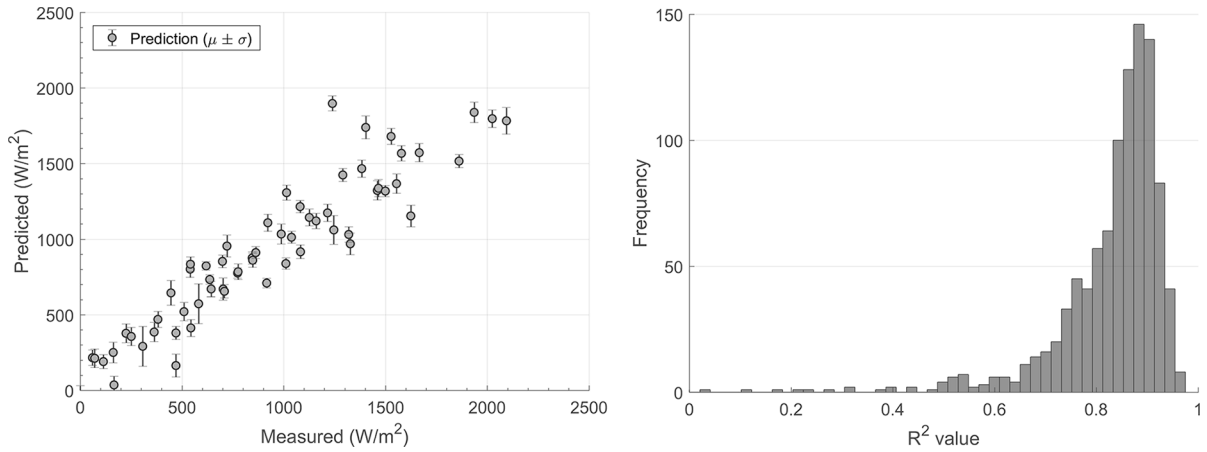

Figure 7. Left: prediction of UV exposure on earlywood spectra from outdoor exposed wood samples. 67% of samples were used to train the model and 33% were used as independent test set. A randomised sampling of the training and test set was performed 1000 times. Right: histogram of R^2 values from the 1000 models.

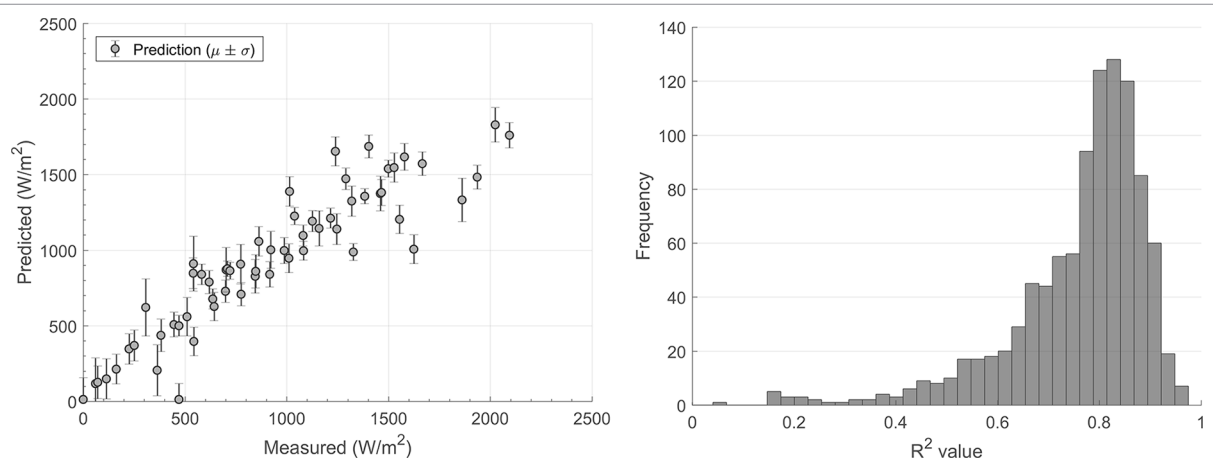

Figure 8. Left: prediction of UV exposure on latewood spectra from outdoor exposed wood samples. 67% of samples were used to train the model and 33% were used as independent test set. A randomised sampling of the training and test set was performed 1000 times. Right: histogram of R^2 values from the 1000 models.

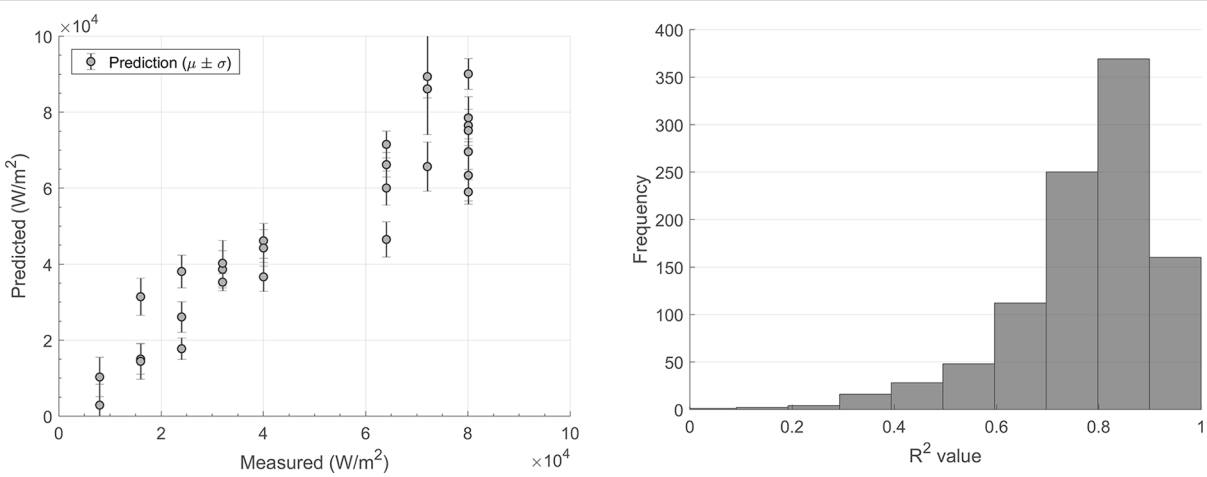

Figure 9. Left: prediction of UV exposure on earlywood spectra from samples in the UV chamber. 67% of samples were used to train the model and 33% were used as independent test set. A randomised sampling of the training and test set was performed 1000 times. Right: histogram of R^2 values from the 1000 models.

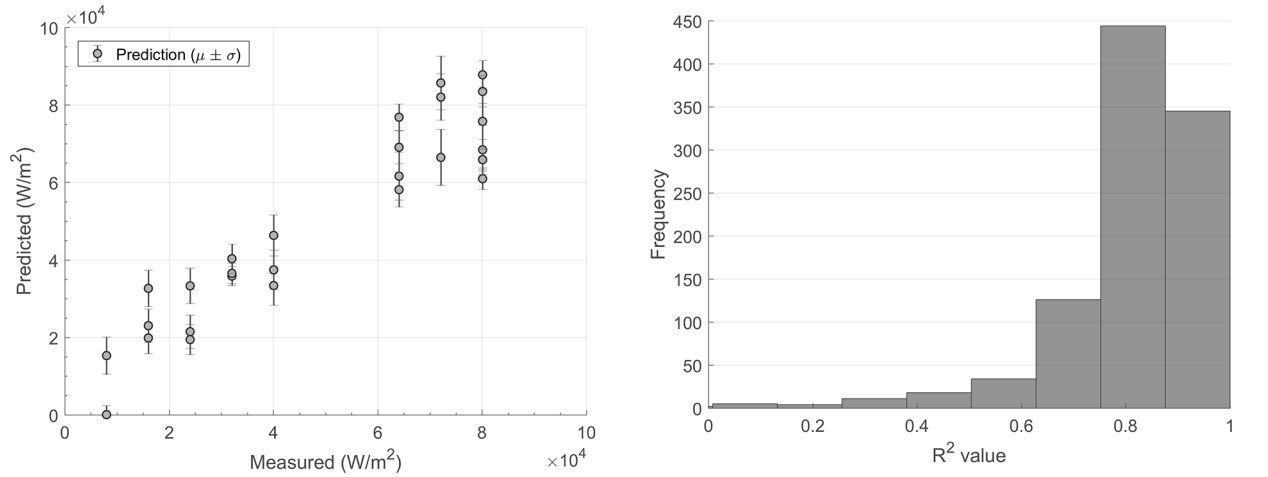

Figure 10 Left: prediction of UV exposure on latewood spectra from samples in the UV chamber. 67% of samples were used to train the model and 33% were used as independent test set. A randomised sampling of the training and test set was performed 1000 times. Right: histogram of R^2 values from the 1000 models.

seen that the UV radiation exposures are of different orders of magnitude for the outdoor and UV chamber exposed samples. For the UV lamp in the UV chamber, only the radiation intensity for the wavelength 340 nm was known, whereas for the outdoor samples the UV radiation is the total integration of the interval between 298 nm and 385 nm. Moreover, additional influencing factors other than UV radiation were present for the outdoor exposed samples, e.g. moisture and temperature, contribute to the degradation together with the UV radiation. The UV radiation is not an independent factor, since the effect of a certain amount of light energy will act differently depending on other climatic factors, as explained in Reference 21.

Chemical analysis

The results from the STA chemical analysis are shown in Table 1. Note that the estimated amount of lignin and holocellulose are given relative to the total weight of the sample. Therefore, although the lignin content seems to increase, this value must be evaluated relative to the mass loss of the sample due to weathering, and the actual lignin content most probably decreases. An experiment using X-rays is planned to estimate the mass loss in early- and latewood separately in order to obtain absolute values for lignin and holocellulose content from the STA measurements. A ridge regression of the early-wood NIR spectra with lignin content as response variable is shown in Figure 12.

Conclusion

Applying NIR hyperspectral imaging along with judicious use of pre-processing and statistical/data mining techniques appears to be a suitable pursuit of understanding and

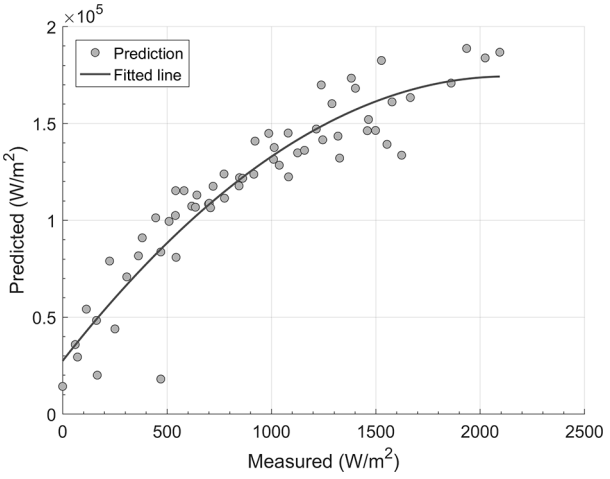

Figure 11. Predictions of UV exposure on outdoor exposed samples using a model that was obtained from the fit of the UV chamber exposed samples using ridge regression.

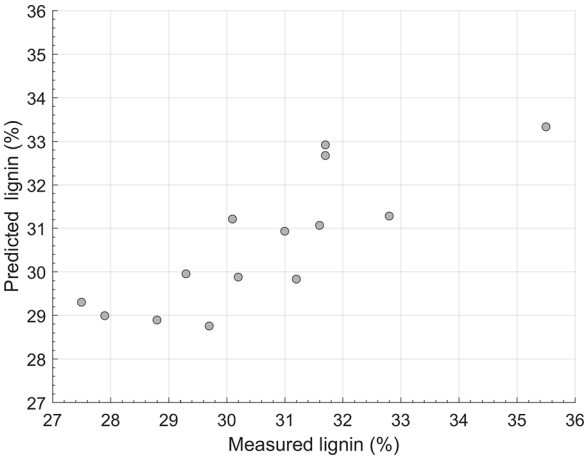

Figure 12. Predictions of lignin content using measured lignin as response variable.

predicting weathering effects on wooden surfaces because it is quick, cheap and non-intrusive. The four different regression models of the NIR dataset all yielded good representations for degradation due to UV exposure. It turns out that shrinking, smoothing or limiting subspace extractions by Tikhonov or PLSR yield very similar prediction accuracies. This is often the case with hyperspectral data, as there are many ways to construct equally accurate and robust regression coefficients. To obtain an improved model for the weathering degradation, additional qualifiers are called for, because the amount of interfering phenomena and their varying intensities undermines the predictive potential of any fitted model to a significant degree. Successfully combining the various factors that constitute the weathering effect into a weather dose will therefore be an important step in this direction. It also appears that if the data used to train the ridge regression model has enough significant outliers, the algorithm can be forced to choose an over-fitted model. While this problem could be addressed and solved by removing the observations from the data set, this severely reduces the number of samples. However, if only some wavelengths are affected while the other wavelengths maintain their predictive power, it might be advantageous to use methods that can perform variable selection (e.g. LASSO or elastic net) and automatically choose the most reliable variables (wavelengths).

The result from the study is a first step towards a weather dose response model determined by temperature and moisture content on the wooden surface in addition to the solar radiation. A weather dosage can be used in combination with microclimate models (such as presented in Thiis *et al.*[3]) as input to simulation tools for architects so that a predicted visual aspects and durability of a façade can be taken into account when planning a building.

Acknowledgements

This work has partly been funded by the Norwegian Research Council in the project "WOOD/BE/BETTER" code 225345 and the project BI04ever (RBSI14Y7Y4) within a call SIR funded by MIUR.

References

1. R.S. Williams, "Weathering of wood", in *Handbook of Wood Chemistry and Wood Composites*, Ed by R.M. Rowell. CRC Press. (2005).
2. L.R. Gobakken, *Surface Mould Growth on Painted and Unpainted Wood; – Influencing Factors, Modelling and Aesthetic Service Life*. PhD thesis, Norwegian University of Life Sciences (2009).
3. T.K. Thiis, I. Burud, D. Kraniotis and L. Gobakken, "The role of transient wetting on mould growth on wooden claddings", in *Proceedings of the 6th International Building Physics Conference, Energy Procedia* 78c, pp. 249–254 (2015). doi: http://dx.doi.org/10.1016/j.egypro.2015.11.629
4. A. Sandak, J. Sandak and M. Riggio, "Assessment of wood structural members degradation by means of infrared spectroscopy: an overview", *Struct. Control Hlth.* **23,** 396–408 (2016). doi: http://dx.doi.org/10.1002/stc.1777
5. G. Agresti, G. Bonifazi, L. Calienno, G. Capobianco, A. Lo Monaco, C. Pelosi, R. Picchio and S. Serranti, "Surface investigation of photo-degraded wood by colour monitoring, infrared spectroscopy, and hyperspectral imaging", *J. Spectrosc.*, Article ID 380536 (2013).
6. M. Schwanninger, J.C. Rodrigues and K. Fackler, "A review of band assignments in near infrared spectra of wood and wood components", *J. Near Infrared Spectrosc.* **19,** 287–307 (2011). doi: http://dx.doi.org/10.1255/jnirs.955
7. D.M. Grossman, *Errors Caused by Using Joules to Time Laboratory and Outdoor Exposure Tests*. ASTM Special Technical Publication 1202, p. 68 (1994).
8. J.H. Kalivas, "Overview of two-norm (L2) and one-norm (L1) Tikhonov regularization variants for full wavelength or sparse spectral multivariate calibration models or maintenance", *J. Chemometr.* **26,** 218–230 (2012) doi: http://dx.doi.org/10.1002/cem.2429
9. A. Savitzky and M.J.E. Golay, "Smoothing and differentiation of data by simplified least squares procedures", *Anal Chem.* **36,** 1627–1639 (1964). doi: http://dx.doi.org/10.1021/ac60214a047
10. H. Martens, J.P. Nielsen and S.B. Engelsen, "Light scattering and light absorbance separated by extended multiplicative signal correction. Application to near-infrared transmission analysis of powder mixtures", *Anal Chem.* **75,** 394–404 (2003). doi: http://dx.doi.org/10.1021/ac020194w
11. A. Kohler, M. Zimonja, V. Segtnan and H. Martens, "Standard normal variate, multiplicative signal correction and extended multiplicative signal correction preprocessing in biospectroscopy". *Comprehensive Chemometrics*, Ed by S. Brown, R. Tauler and R. Walczak. Vol. 2. Elsevier, Oxford, pp. 136–162 (2009). doi: http://dx.doi.org/10.1016/B978-044452701-1.00102-2
12. Q. Li, O. Gao and G. Zhang, "Improved extended multiplicative scatter correction algorithm applied in blood glucose noninvasive measurement with FT-IR spectroscopy", *J. Spectrosc.* Article ID 91635 (2013).
13. D.C. Lay. *Linear Algebra and its Applications*, 4th Edn. Pearson (2012).
14. T. Hastie, R. Tibsharani and J. Friedman, *The Elements of Statistical Learning. Data Mining, Inference and Prediction*, 2nd Edn. Springer (2008).
15. A.E. Hoer and W.K. Robert, "Ridge regression: biased estimation for nonorthogonal problems". *Technometrics* **12,** 55–67 (1970). doi: http://dx.doi.org/10.1080/00401706.1970.10488634

16. P.C. Hansen, "Analysis of discrete ill-posed problems by means of the L-curve", *SIAM Review* **34,** 561–580 (1992). doi: http://dx.doi.org/10.1137/1034115

17. S.-J. Kim, K. Koh, M. Lustig, S. Boyd and D. Gorinevsky, "An interior-point method for large-scale 1 1-regularized least squares", *Sel. Top. Signal Process.* **1,** 606–617 (2007). doi: http://dx.doi.org/10.1109/JSTSP.2007.910971

18. F. Stout, J.F. Kalivas and K. Héberger, "Wavelength selection for multivariate calibration using Tikhonov regularization", *Appl. Spectrosc.* **61,** 85–95 (2007). doi: http://dx.doi.org/10.1366/000370207779701479

19. S. Wold, M. Sjöström and L. Eriksson, "PLS-regression: a basic tool of chemometrics", *Chemometr. Intell. Lab. Syst*. **58,** 109–130 (2001). doi: http://dx.doi.org/10.1016/S0169-7439(01)00155-1

20. L. Eldén, *Matrix Methods in Data Mining and Pattern Recognition*. SIAM (2007). doi: http://dx.doi.org/10.1137/1.9780898718867

21. A. Krishnan, K. Lynne, J. Williams, A.R. McIntosh and H. Abdi, "Partial least squares (PLS) methods for neuroimaging: a tutorial and review", *Neuroimage* **56,** 455–475 (2011). doi: http://dx.doi.org/10.1016/j.neuroimage.2010.07.034